

Characterization of the surface and mechanical properties of the friction stir welding in tri-dissimilar joints with aluminum alloys and titanium alloy

S. Delijaicov¹ · D. Y. Yakabu¹ · B. De Macedo¹ · H. B. Resende² · M. H. F. Batalha²

Received: 17 July 2017 / Accepted: 1 November 2017 / Published online: 10 November 2017
© Springer-Verlag London Ltd., part of Springer Nature 2017

Abstract The search for lighter and more resistant structures contributed to the development of effective welding methods. Among them, friction stir welding, a recent technique patented in 1991, in which welding is performed by the friction between a rotating tool and the materials to be welded, has widely been studied in the last decades. Among the advantages the technique provides, are the possibility of welding aluminum alloys series 2xxx and 7xxx, and the possibility of welding materials of different chemical compositions. The industry is still cautious about using this technique, yet several studies have been performed to improve knowledge on it. This research investigated the three dissimilar junctions between aluminum alloys 2024-T4 and 7475-T6 with titanium alloy Ti6Al4V. The aluminum alloys were positioned on the top portion of the welding creating a butt weld. The titanium alloy was placed on the bottom portion of the weld creating a lap welding with the aluminum alloy. The parameters of rotation, welding speed, and tilt were varied, following a central composite experimental design. Through the response surface analysis, it was possible to identify the correlation between the input and output parameters. This correlation is used to identify main influence between the parameters and can be used to optimization of the process. The influences of these parameters were evaluated on the welding surface by measuring residual stress and microhardness. The residual stress was

analyzed by the hole drilling method on the aluminum side and by X-ray diffraction on the titanium side. The microhardness was analyzed by the Vickers test. On the aluminum side, residual stress and microhardness show a strong relation; high value of residual stress resulted in low value of microhardness. On the titanium side, residual stress shows a relation with temperature; the high value of temperature resulted in low value of stress. The tensile test was used to compare joint efficiency between different welding parameters and the base metal. It was possible to reach parameters in which the welding ultimate tensile stress exceeded the AA2024 value.

Keywords Friction stir welding · Residual stress · Microhardness · Tri-dissimilar junction

1 Introduction

One of the great challenges of the mobility industry is the search for advancing the energy efficiency of its products, contributing to the reduction of pollutant emission and ensuring the competitiveness of the evolution of the market and the technology, as reported by Mishra and Ma [13].

In the automotive industry, regulatory agencies around the world limit the emission of pollutants from vehicles as well as the aeronautics industry, abiding by the International Civil Aviation Organization.

One of the solutions adopted to improve these parameters focuses on mass reduction. In the automotive sector, for every 100 kg of mass reduction, 9 g of CO₂ per kilometer is reduced (European Aluminum Association [4]). In aerospace vehicles, only 5% of the weight of the aircraft is destined to payload. The largest portion of this mass is used in structural components and fuel. Mass reduction would represent a higher load capacity [15].

✉ S. Delijaicov
sergiode@fei.edu.br

¹ Mechanical Engineering Department, Centro Universitário FEI, São Bernardo do Campo, SP, Brazil

² Laboratório de Estruturas Leves do Instituto de Pesquisas Tecnológicas do Estado de São Paulo, São José dos Campos, SP, Brazil

Different materials are employed in FSW to achieve significant mass reductions. Aluminum and its alloys are materials widely used because of their low density compared to the steels usually employed, as reported by Rodriguez et al. [16], Guo et al. [5], Cavaliere et al. [2], Song et al. [19], and Khodir and Shibayanagi [8]. Titanium and its alloys are another widely used material, mainly in the aeronautical and naval industry, as an alternative for mass reduction [1, 11, 12]. Its relation between weight and mechanical properties is favorable to numerous applications. The excellent mechanical properties at high temperatures favor the use of titanium, mainly in turbines used in the aerospace industry.

The FSW welding process allows joining similar and dissimilar metals since it is considered a soldering process in the solid state, i.e., it does not involve melting materials. The process, initially applied to aluminum, was invented by Thomas et al. [20] consisting of a non-consumable, rotary tool applied at the junction of the parts to be welded. As the weld is consolidated, the tool moves in the direction of the feed and, due to friction and rotation, the contact region undergoes sufficient heating so that the metals plasticize and mix together ([11, 12]).

Boeing's defense systems division used the FSW technique in the Delta II and IV programs for manufacturing rocket fuel tanks, achieving cost savings of 20% in relation to rivet fixing, as well as a significant reduction in the construction time. The Catamaran, built by Marine Aluminum A. S., is another example of the technique application used for constructing its panels, reported by Shah and Tosunoglu [17].

The FSW technique began to be used for mass producing automotive vehicles by Honda Motors Corporation in 2012 in the production of the Accord 2013 vehicle at the Ohio plant in the USA, reported by Kusuda [10].

The union of three dissimilar metals was studied. Two aluminum alloys (AA5083 and AA6061-T6) were welded with steel using a single soldering pass FSW, making it possible to obtain a weld with 73% bonding efficiency [7].

Copper welding with stainless steel was studied by [14]). The dominance of ductile fracture was observed, with a yield stress of 85% of the base material with lower flow stress.

Salih et al. [18] used FSW in composite aluminum matrices, denominated aluminum matrix composite in the literature. He obtained better results than with conventional laser and tungsten inert gas.

Several studies involving the joining of aluminum alloys with titanium alloys have been presented over the years. The interest lay in the creation of structures with reduced weight, balancing the low density of aluminum with high hardness, resistance to corrosion, and good properties at high temperatures of titanium. This made the aerospace and automotive industries the main stakeholders.

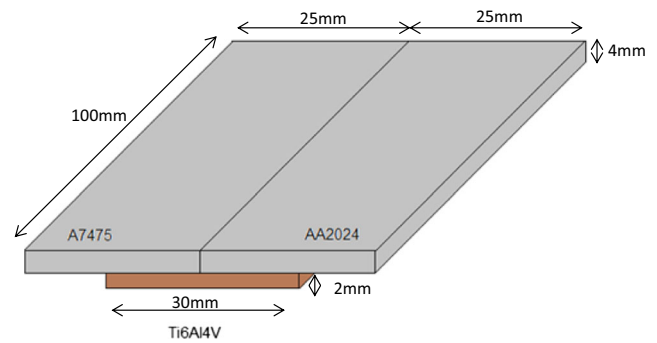


Fig. 1 Layout of the plates. Source: author

In the studies of joining titanium alloys with aluminum in the top weld, the generation of $TiAl_3$ is the most relevant factor for the quality of the weld. It is a brittle characteristic composition, and therefore an excessive formation is not desired, for example with a thickness above $5 \mu m$ [9].

The formation of the $TiAl_3$ layer occurs when the FSW process reaches a pressure and temperature condition, at the interface between Ti and Al, favorable for the reaction. Hence, the high pressure ruptures the oxide layer of the plates, allowing the contact between Al and Ti. After the contact, due to the temperature, the reaction occurs and forms $TiAl_3$ [3].

As well as the properties of the tools, the test parameters play a major role in weld quality. Its influences are directly linked to the heat generated between the tool and the parts, and

Table 1 Test parameters

Test	Specimen	Rotation (rpm)	Travel speed (mm/min)	Tilt angle (°)
1	25	1100	20	1
2	7	1500	20	1
3	24	1100	40	1
4	8	1500	40	1
5	10	1100	20	3
6	9	1500	20	3
7	17	1100	40	3
8	22	1500	40	3
9	26	1300	30	0.32
10	23	1300	30	3.68
11	11	1300	13.18	2
12	13	1300	46.82	2
13	20	963.6	30	2
14	12	1636.4	30	2
15	15	1300	30	2
16	14	1300	30	2
17	16	1300	30	2
18	19	1300	30	2
19	18	1300	30	2
20	21	1300	30	2

Source: author

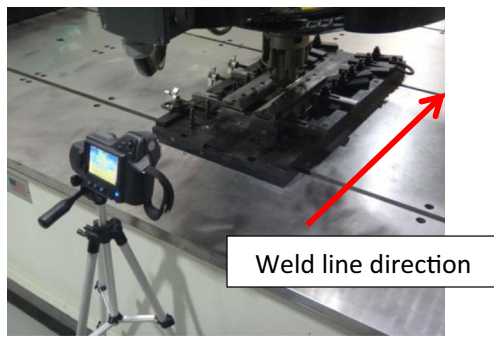


Fig. 2 Camera position to temperature surface measurement. Source: author

are suitable according to the tool used and the properties of the material to be welded. Five basic parameters are controlled: tool rotation; tool feed (translation movement); axial force; tool angle or tilt; penetration.

Motivated by the study on FSW in tri-dissimilar junctions, our aim is to search for a junction of AA2024-T4 aluminum alloys, AA7475-T6, and Ti-6Al-4V titanium. These materials are usually used on aeronautic industry and have limitation on conventional welding techniques. The study was based on the variation in the main parameters of solder to identify characteristics inherent to the process. Surface evaluation was performed by analyzing residual stress and surface microhardness. For measuring the residual stress, the blind hole and X-ray diffraction techniques were used. The microhardness was evaluated on the Vickers scale and the mechanical properties were evaluated by the tensile test. Microstructural characterization was performed by optical microscopy and SEM.

2 Methodology

The materials used for the study were aluminum alloys AA2024-T4 and AA7475-T6, and titanium alloy Ti6Al4V. The 4-mm-thick aluminum plates were cut in the dimensions of 25 mm by 100 mm, and the 2-mm-thick titanium plates were cut in the dimensions of 30 mm by 100 mm.

The aluminum plates were secured to form a top weld, while the titanium plate was secured beneath the aluminum plates, forming an overlapping weld. The position of the aluminum plates was arranged so as to maintain the AA2024 alloy in the advancing position and the AA7475 alloy in the retreating position according to Fig. 1.

The tool was made with H13steel in the dimensions of 20 mm of shoulder diameter by 80 mm in length. The pin had a diameter of 5 mm at the tip and 6 mm at its base and the length was 4.0 mm.

After the tool was machined, the vacuum tempering and tempering process was carried out, and the tool was then subjected to nitriding. Fifteen tools were made for the study.

For the experiment, a central rotational composite plan was used with five replicates at the central point. Three independent variables were used with two levels of variation. These levels were determinate after a previous experience with a wide range of parameters, and these were the values which the welding were consolidated. The complete experiment test is shown in Table 1.

The complete planning consisted of 20 trials. At the time of the test execution, the order was randomized to prevent biasing the results. Statistical analysis of the results was performed by the STATISTICA software, version 12 (Statsoft Inc.). It was used to analyze

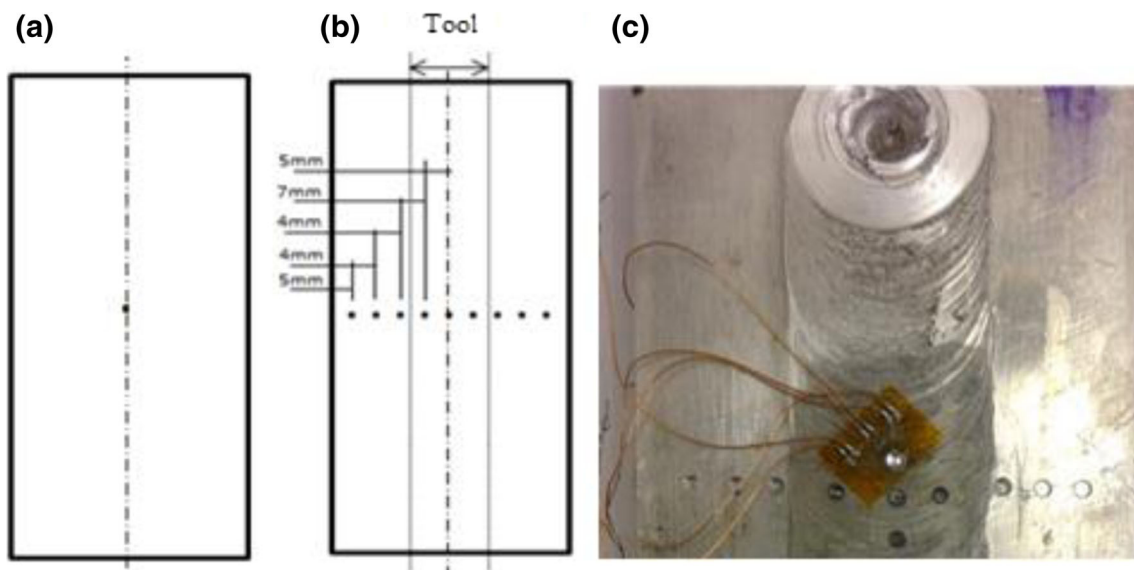


Fig. 3 Layout of the extensometers: **a** measurement point in the weld line and **b** measurement points of the cross section, and **c** strain gauge attached to the aluminum plate. Source: author

Pareto graphic and response surface. Pareto graphic show the influence of each input parameter with the output parameter in study and the response surface give a visual image of how the parameters affect the response. These results are useful to identify relevant parameters to active desire output on the process.

The welding was carried out in the premises of the Institute of Technological Research (IPT) of São José dos Campos, using the Manufacturing Technology, Inc. machine. The machine has five axes, a 2000 mm × 1500 mm × 800 mm work table, maximum load axial displacement of 80 kN, maximum rotation of 300 rpm, and maximum feed of 3000 mm/min. The machine head is equipped with load cells to measure welding forces and torque.

An initial feed of 10 mm/min was used to avoid defect formation.

At each test, the conditions of the tool were checked. In case a change of more than 1 mm in the length or thickness of the pin diameter was detected, the tool was replaced.

Microscopic analysis was performed using scanning electron microscopy (SEM) of CamScan, model CS3200LV, of the FEI Materials Laboratory.

The transverse region of the weld was analyzed to identify the behavior of the mixture between the aluminum alloys and the titanium alloy. Two conditions were evaluated. Specimen 22 showed no tool contact on the titanium plate, while specimen 24 presented the tool contact with the titanium plate.

The surface temperature of the process was measured by a Flir T450sc thermal camera. The camera was positioned at 400 to 500 mm from the region of the weld seam in the back side in the same direction of the weld line as show on Fig. 2. The temperature was analyzed with the mean of the maximum temperatures recorded during the study time interval.

Surface residual stress analysis was performed using the X-ray diffractometer from the FEI university center materials laboratory. The diffractometer used was a Shimadzu model XRD-7000. The measurements used a copper tube with nickel filter, indicated for titanium measurements. The coefficient related with the stress necessary to diffraction peak according the specimen material called K factor used was $-254.5 \text{ N/mm}^2/^\circ$ with an angle of 141.7° .

Measurements were made on the underside of the specimen, in the region of the titanium plate. All the measurements were made in the longitudinal direction of the weld.

The surface stress analysis of the upper side was performed by the blind hole technique because the superficial imperfections resulting from the weld prevented the use of the X-ray diffraction technique. To

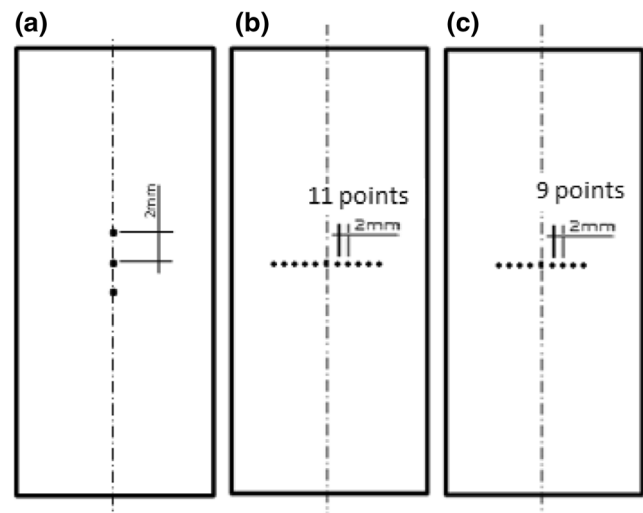


Fig. 4 Microhardness measurement points. **a** weld line, **b** cross-sectional profile on aluminum surface, and **c** cross-sectional profile of titanium surface. Source: author

standardize the weld region, a thin layer of self-polymerizing resin composed of methyl ethyl methacrylate copolymer, pigments, and peroxide was applied.

The measurement used extensometer rosettes, Excel type PA-13-060RF-120L. The pitch drill used was SINT, model MTS 3000, with a tapered milling cutter of 1.8 mm in diameter. To prevent the wear of the milling cutter from interfering with the measurements, the milling cutter was replaced every two holes.


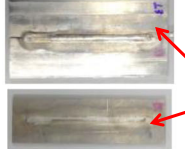







Initially, a drill was made until the cutter drilled the resin and reached the specimen. From this point, a penetration of 0.3 mm was assumed for eliminating the burr layer resulting from the welding process.

After the bore preparation process, the measurement was performed up to a penetration of 0.6 mm, at intervals of 0.03 mm. The data were collected by the software Residual Stress Measurement System version 5.3.1 and treated in the software Hdrill version 3.01,



Fig. 5 Cut of traction specimens by wire electrodes. Source: author

Fig. 6 Defects summary. Source: author

Test	Specimen	Rotation [RPM]	Travel speed [mm/min]	Tilt angle [°]	Defect	Photo
10	23	1300	30	3.68	Detachment of the titanium plate	
12	13	1300	46.82	2	Detachment of the titanium plate	
12	13	1300	46.82	2	Surface crack	
14	12	1636.4	30	2	Burr	
15	15	1300	30	2	Burr	
17	16	1300	30	2	Burr	
8	22	1500	40	3	Burr	
4	8	1500	40	1	Superficial void	
9	26	1300	30	0.32	Interior voids	

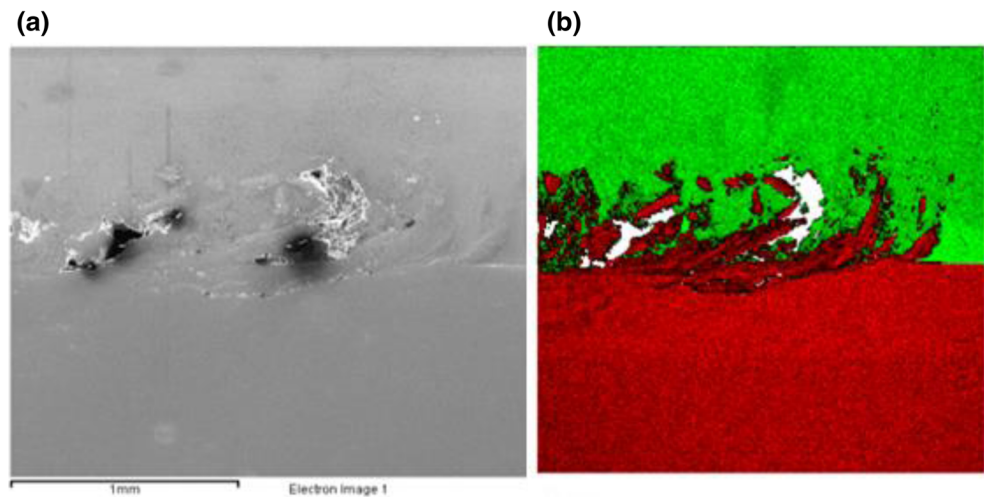
using the Integral Method to calculate the residual stresses.

The residual stress in the weld line was measured for all specimens. Item (a) of Fig. 3 shows the region where the stress was measured. In specimens 8 and 17, the cross-section was measured at nine points spaced apart according to item (b), and item (c) of Fig. 3 shows the drilling points for the cross-section and the strain gauge fixed in the region of the weld line.

Microhardness was measured with a Shimadzu microhardness meter model HMV-2. The Vickers microhardness was used, with a load of 4.903 N.

The microhardness was evaluated in the weld line of all the specimens in the upper and lower region of the weld. Three measurements were performed and, for the statistical analysis, the mean was used among these measures. Figure 4 item (a) illustrated the points of measurement on weld line.

Fig. 7 Image of specimen 24 in the region between the aluminum plates and the titanium plate where the tool was contacted. **a** Untreated image and **b** EDS image. Source: author



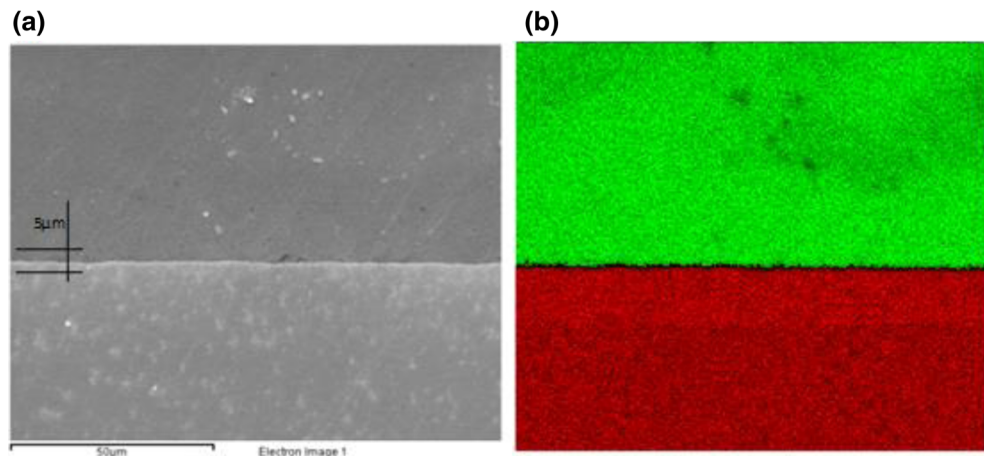
The cross-sectional profile on the surface of aluminum side and titanium side (located in the upper and lower regions of the weld) was evaluated in specimens 8 and 17 as a function of the distance of the weld line. It was done with 11 measurements made 2 mm apart from each point on the aluminum side and 9 points on the titanium side. The Fig. 4 items (b) and (c) illustrated the points of measurement along the cross-section.

Microhardness was measured on an Olympus BX60M microscope coupled with an Olympus SC30 camera. For measuring and calculating microhardness, AnalySIS software version 5.1 of Olympus Soft Imaging Solutions GmbH was used.

For the tensile test, a Material Test System MTS 810 machine was used and the test speed was 2 mm/min. The resistance limit was measured on all specimens.

The specimens were cut by wire electrodes, fixed by one side of the specimen as illustrated in Fig. 5. The measurements of the specimen followed ASTM E8/E8M-15A. The specimen head was reduced to fit the size of the welded plates. Two tensile specimens were removed from each plate.

Fig. 8 Image of specimen 22 in the region between the aluminum plates and the titanium plate where the tool was contacted. **a** Untreated image and **b** EDS image. Source: author



In addition to the welded test specimens, three test specimens of the AA2024-T4 and AA7475-T6 alloys were tested without further processing for further comparison of weld efficiency.

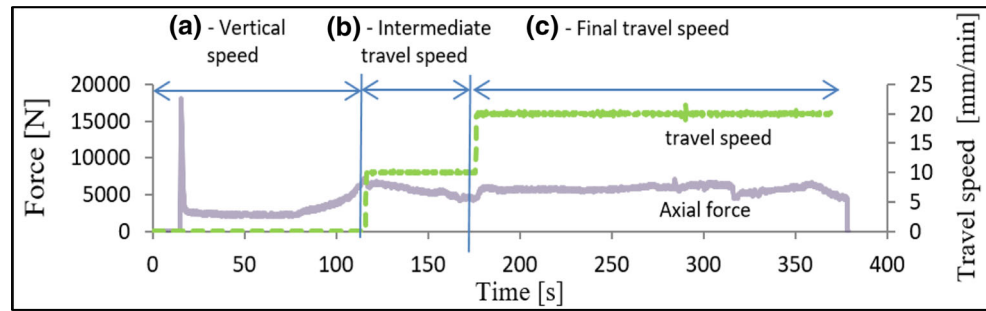
3 Results and discussions

3.1 Identification of defects

All the specimens were visually inspected to detect usual weld defects such as voids, burrs, or cracks. All defects founded are summarized in Fig. 6.

Specimens 13 and 23 showed the detachment of the titanium plate after the welding process. Specimen 23 was processed at an angle of 3.68° . Due to the tool calibration method, the higher the angle of inclination, the lower the penetration of the pin in the aluminum plate. Hence, the penetration of the tool was not enough to consolidate the joint of the titanium plate. In specimen 13, the feed rate of 46.83 mm/min was very high and may have been the cause of the joint not being

Fig. 9 Supporting axial thrust force of the specimen 25. Source: author



consolidated. According to Najafkhani et al. [14], high feed causes insufficient heat supply, generating a defective solder.

Burr formation was found in most of the specimens on the feed side. Specimens 12, 15, and 16 showed excessive burr on the feed side.

Specimen 22 showed excessive burr on both sides of the weld. The parameters of the test were 1500 rpm, feed of 40 mm/min, and angle of 3°.

A superficial void defect was found at the beginning of the weld of specimen 8. This region corresponds to the transition of the intermediate and final advance of the test. The parameters of the test were 1500 rpm, advance of 40 mm/min, and angle of 1°. After the surface treatment for the microhardness

test, it was possible to verify the existence of a crack below the surface void region. The formation of voids is related to inadequate welding parameters, linked to rotation and excessive advance [9]. In the case of specimen 8, the rotation and advance parameters were the maximum level of the experimental design.

In specimen 13, after the surface treatment for microhardness, a crack in the weld was also identified on the feed side. In this specimen, the feed rate was 46.83 mm/min, possibly causing the formation of an inadequate mixture and the formation of the crack.

Specimen 26 showed a lack of contact of the shoulder with the surface of the aluminum plates. This test presented the

Table 2 Results of the support axial thrust force, torque, temperature, and residual stress

Test	Specimen	Rotation (RPM)	Travel speed (mm/min)	Tilt angle (°)	Axial force (N)	Torque (N·m)	Temperature (°C)	Residual stress (MPa)
1	25	1100	20	1	5832.85	16.89	361.61	154.00
2	7	1500	20	1	4583.66	13.51	388.31	117.00
3	24	1100	40	1	6515.01	17.47	359.84	105.00
4	8	1500	40	1	6180.45	14.23	414.39	130.00
5	10	1100	20	3	4041.32	15.03	349.51	346.00
6	9	1500	20	3	3936.13	12.47	327.94	219.00
7	17	1100	40	3	5258.00	16.64	372.17	159.00
8	22	1500	40	3	5102.20	13.34	404.95	87.00
9	26	1300	30	0.32	3807.02	13.17	323.39	49.00
10	23	1300	30	3.68	5659.85	15.71	358.98	218.00
11	11	1300	13.18	2	4506.85	14.84	397.75	317.00
12	13	1300	46.82	2	5751.05	15.68	351.25	-24.00
13	20	963.6	30	2	5481.29	17.08	356.66	138.00
14	12	1636.4	30	2	4746.64	14.74	397.50	194.00
15	15	1300	30	2	5886.85	15.40	366.02	177.00
16	14	1300	30	2	4215.21	14.70	389.31	57.00
17	16	1300	30	2	5200.68	15.38	369.89	344.00
18	19	1300	30	2	5443.92	14.67	321.30	92.00
19	18	1300	30	2	5522.52	15.17	384.59	24.00
20	21	1300	30	2	5358.57	15.18	368.48	338.00

Source: author

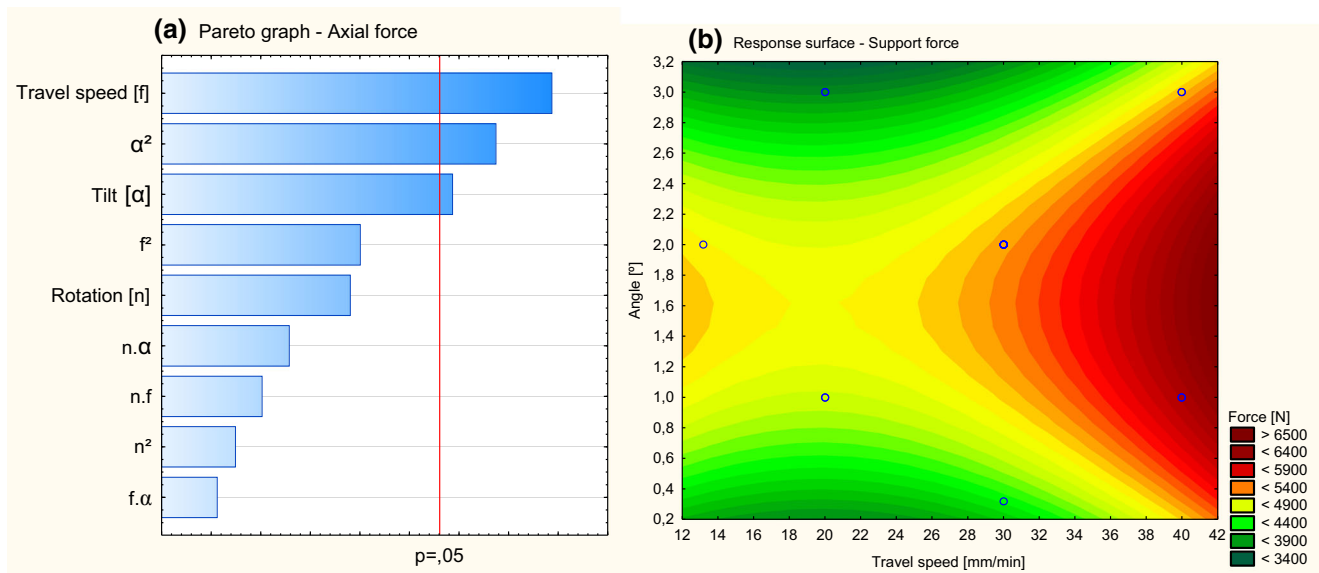


Fig. 10 **a** Pareto graph in the analysis of the support force and **b** response surface of support force. Source: author

lowest angle of the experimental design, 0.32° . Due to the low angle, the shoulder penetration in the aluminum plate was inadequate, causing an irregular flow of the plasticized metal on the surface and reaching low temperature, resulting in an inadequate mixing.

By evaluating the cross-sectional profile of the weld, it was possible to identify the formation of voids in some test parameters. Among the tests, specimen 26 showed the largest void. The same test specimen presented an irregular mixture on the surface due to inadequate parameters. According to Hiller [6], the defect is linked to inadequate welding parameters.

After the cross-section of the specimens, the touch of the tool was identified on the titanium plate in specimens 7, 8, and 24. The mixture between the elements could be observed in the mixing zone, near the interface of the plates. In all the specimens, which had contact with the titanium plate, the tool angle was 1° . This was due to the method of tool height calibration, in which the lower the tool tilt angle, the greater the penetration of the pin in the weld.

3.2 SEM

The touch of the tool on the titanium plate promoted the mixing between titanium and aluminum. In Fig. 7, the green region represents the aluminum and red, the

titanium. The mixture was not efficient and resulted in the formation of internal voids, represented by the white region in the figure, which resulted in low efficiency in the tensile test.

In specimen 22, where there was no contact of the tool with the titanium plate; the region between the titanium and the aluminum did not show a mixture between the elements, as shown in Fig. 8. Neither also, the formation of the intermetallic layer more than $5 \mu\text{m}$ between base metals.

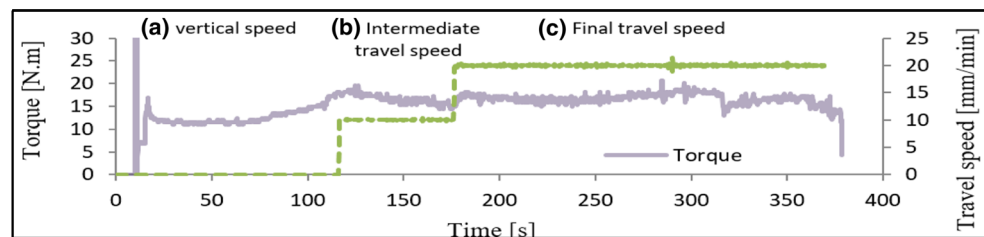
3.3 Supporting force (F_z) analysis

Figure 9 shows the behavior of the support force for 1100 rpm, advancement of 40 mm/min, and angle of 1° in specimen 25.

In region (a), the insertion of the tool occurred in specimen 25, where at the initial moment, a high force is observed. The maximum force observed was 18 kN for 1110 rpm, advance of 20 mm/min, and angle of 1° . The high force results from the first contact of the tool with the specimen, the temperature of which is still low.

Immediately after the penetration of the tool, this force is reduced to a minimum value. In this region, the minimum value was 1.3 kN for 1636.4 rpm, feed of 30 mm/min, and angle of 2° . This reduction is due to the decrease in the resistance of the movement, the heating of the region, and,

Fig. 11 Register of the torque in the region of horizontal movement for specimen 25. Source: author



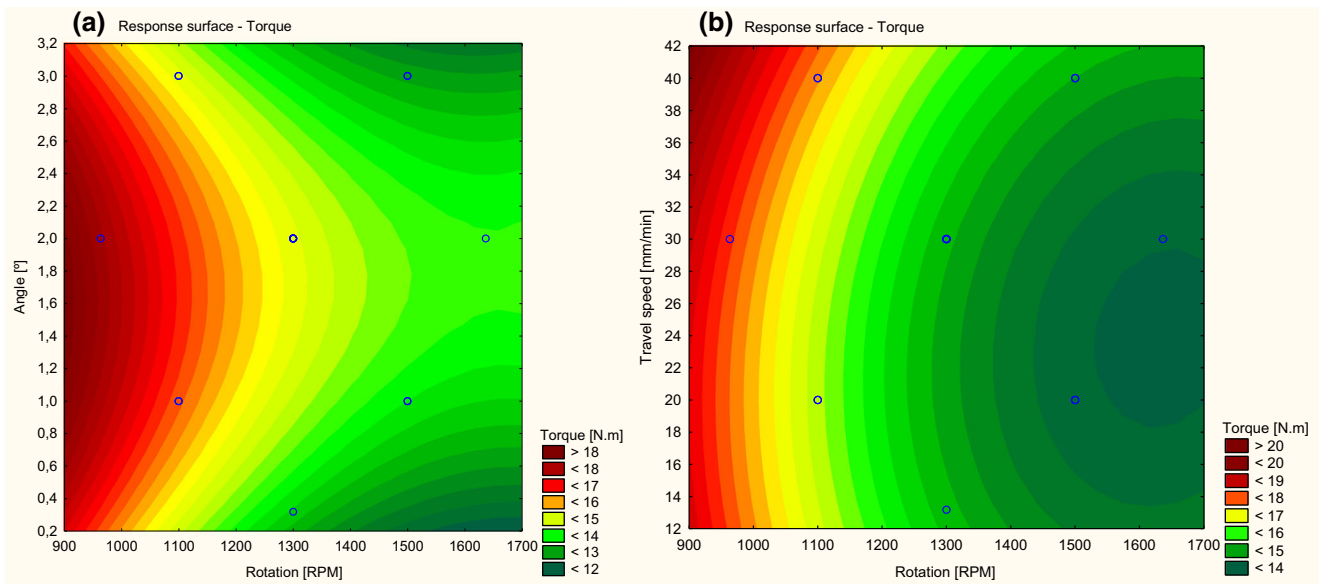


Fig. 12 Response surface **a** angle × rotation and **b** travel speed × rotation. Source: author

consequently, the alteration of the state of the material which has a favorable environment for mixing. An increase in the force at the end of the vertical movement is noticed due to the contact of the shoulder with the plates to be welded.

In region (b), the tool starts the process of displacement toward the weld. To avoid a sudden change of welding conditions in this region, the feed used was intermediate to the desired final feed. It is possible to observe a peak of force at the beginning of the movement, which decreases slightly during the movement.

In region (c), the tool starts to operate on the parameters planned for the experiment. A small oscillation of the stress is observed at the beginning of the region due to the change in the feed direction, and near the end of the specimen due to the proximity of its end. In this region, the maximum force observed was 6515 N for

specimen 24 and the minimum force was 3807 N for specimen 26. Table 2 shows the results in region (c) of all the parameters tested.

The statistical analysis of the data resulted in a R^2 of 0.73. The parameters of greatest influence were advancement and angle. The Pareto graph shown in Fig. 10 item (a) shows the relationship of all the independent parameters to the bearing force.

By analyzing the response surface of Fig. 10 item (b), between the two parameters of greater influence, the feed and the angle, an increase of the feed was observed to result in an increase of the support force, whereas the angles between 1.4° and 1.8° presented the greatest support force. High angles resulted in lower pin penetration and, consequently, lower supporting force was observed. Minor angles (0.32°) presented

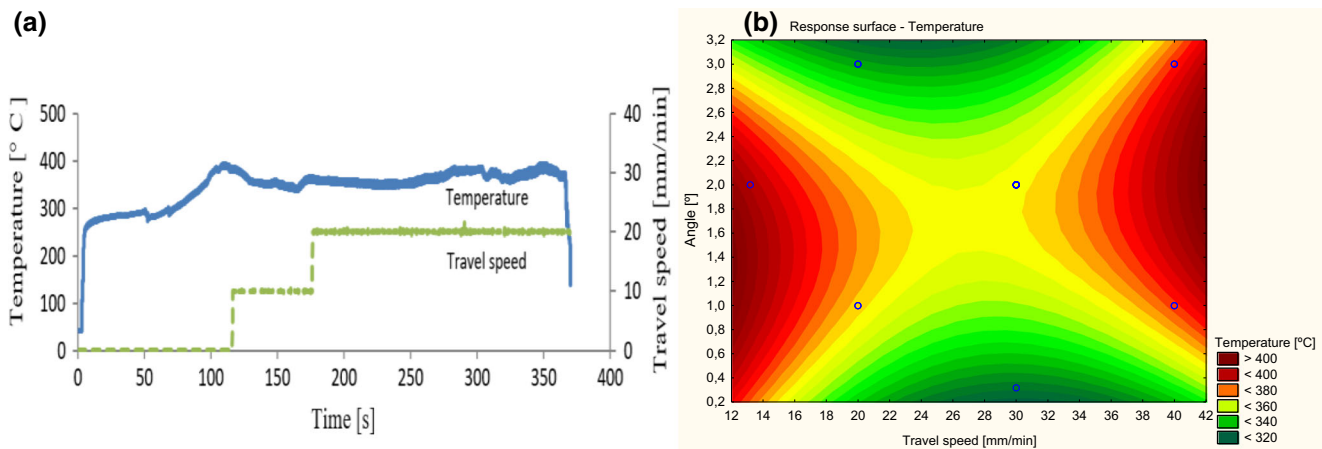


Fig. 13 **a** Register graph of temperature variation over time of specimen 25 and **b** response surface. Source: author

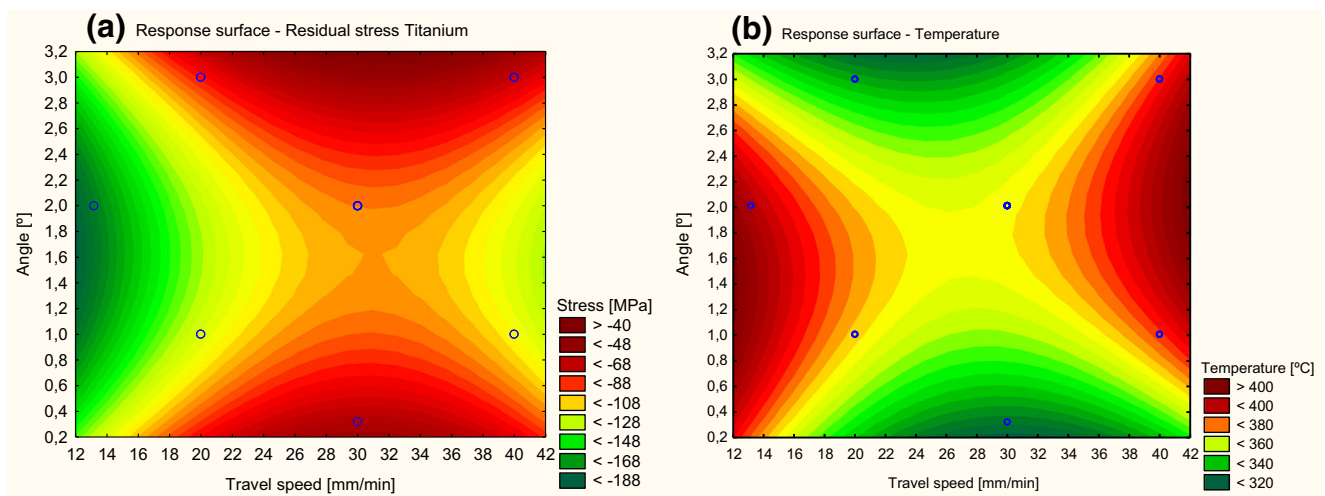


Fig. 14 Response surface between angle and travel speed. **a** Residual stress and **b** temperature. Source: author

inadequate mixing, such as void formation inside the weld, influencing the resulting supporting force. According to Kim et al. [9], high feeds favor the low heat supply and, consequently, the plastic metal region is reduced. This resulted in the increase of the force required to maintain the positioning of the tool in the welding process.

3.4 Torque analysis

The torque was evaluated according to the three stages of the welding process, according to Fig. 11. In the first step, a torque peak with up to 377 Nm was observed for 1500 rpm, feed of 20 mm/min, and angle of 1°, according to the configuration of the test in specimen 25. This peak is related to the contact of the tool with the specimen.

After the peak torque, the value decreases to a minimum of 3.87 N·m and begins to increase again due to the shoulder contact. When the horizontal movement starts, a slight increase in torque is observed, which decreases until the feed is changed again, this time to

the value of the test. During the final feed, a decrease in torque is observed, close to the end of the specimen.

The statistical analysis obtained a R^2 of 0.89. The three independent parameters showed a correlation with the torque, the rotation of which was the parameter of best relation, followed by the angle and the feed.

The response surface between the rotation and the angle on Fig. 12 showed that the maximum torque is in low rotation. According to Kim et al. [9], low rotation is related to low heat supply. A low temperature resulted in a reduced plasticized metal region and, consequently, a greater resistance to tool movement. The influence of the angle is more noticeable at high rotations, in which angles close to 2° presented higher torque. However, its influence is low compared to the influence of rotation. As with the supporting force, high angles showed low penetration and smaller angles resulted in a defect in the weld.

The response surface obtained between the angle and the feed showed that the angle between 1.4° and 1.6° show the highest torque. High angles resulted in less tool penetration and smaller angles resulted in

Fig. 15 Profile of the longitudinal residual stress at different distances of the weld line—titanium side. Source: author

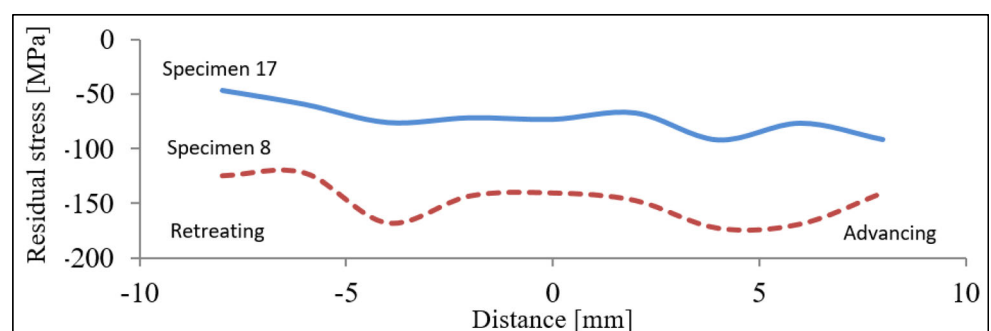
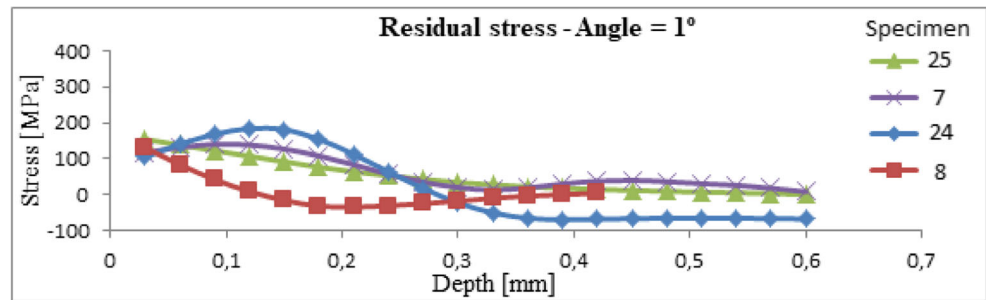


Fig. 16 Surface residual stress for conditions with angle = 1°



uneven mixing. The advancement showed an opposite behavior; the central region between 24 and 28 N·m presented the region of lower torque. The torque showed a behavior similar to the support force.

3.5 Temperature analysis

Figure 13 item (a) illustrates the temperature behavior over time of specimen 25. In the first step, corresponding to the penetration of the tool, a rapid increase in temperature was observed, reaching about 260 °C. After the tool penetration, the temperature increased at a slower rate, reaching the peak of temperature, with the onset of the horizontal movement, of approximately 380 °C. From this step, the temperature is stabilized throughout the weld. A small variation is observed due to the forward transition.

The analysis in ANOVA showed a R^2 of 0.76; the advance and the angle presented a p significance level lower than 0.05. The surface response Fig. 13b show obtained between the feed and the angle showed that the temperature obtained is high for extreme feedings greater than 36 mm/min or less than 18 mm/min. Conversely, extreme angles had low temperatures. Just as in the axial support force and the torque, extreme angles resulted in a lower penetration and at smaller angles, an irregular mixture occurred. Low feeds favor the supply of heat and high feeds, due to favoring high axial supporting force and high torque, also favored for elevated temperatures.

3.6 Titanium longitudinal residual stress

The residual stress in the lower part of the weld presented a compressive behavior in all the specimens. One possible explanation would be that the sheet is drawn in the aluminum region and, consequently, compressive in the titanium region. The highest stress obtained was - 52.48 MPa for the parameters 1300 rpm, 30 mm/min of feed, and 0.32° angle, and the lowest stress observed was - 164.71 MPa for 1300 rpm, feed of 13.18 mm/min, and angle of 2°.

The analysis in ANOVA showed a R^2 ratio of 0.76, in which the feed and angle were the parameters of better relationship with the residual stress.

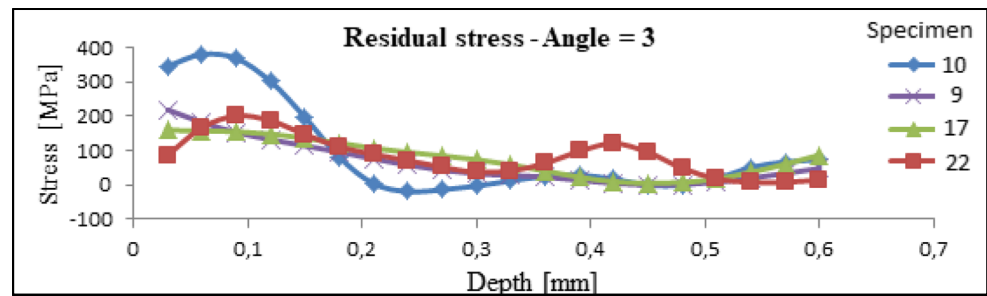
The response surface between the angle and the feed on Fig. 14 shows that extreme feed rates present higher residual stress, while extreme angles have low residual stress. By comparing the response surfaces of the residual stress and temperature, the inverse relationship between them can be noted. In regions with elevated temperature, the residual stress was smaller and in regions with low temperature, the stress was greater. The same relationship between temperature and residual stress was observed [21]), and it is attributed to the higher temperatures obtained, the appearance of a more uniform gradient, and, consequently, a reduction in deformation and residual stress. Despite the same relation, Chen and Nakata [3] attributed the greater influence of the residual stress to the rotation. The tool format and the test parameters can be one of the factors of the difference in the result in relation to the parameter of greatest influence.

Table 3 Resume of the welding parameters for Fig. 16

Test	Specimen number	Rotation, n (rpm)	Travel speed, f (mm/min)	Tilt angle, α (°)
1	25	1100	20	1
2	7	1500	20	1
3	24	1100	20	1
4	8	1500	20	1

Source: author

Fig. 17 Surface residual stress for conditions with angle = 3°



The behavior of the residual stress at different distances of the weld line is shown in Fig. 15. In specimen 8, an increase in stress was observed from the center point to the ends of the tool pin, located 2.5 mm from the zero point. From 2.5 to 4 mm from the center, a stress drop occurred, and from 4 to 6 mm from the center, a stress rise occurred. In the central region, the increase of the residual stress is related to the contact of the pin with the titanium plate, which, besides the mechanical work, caused elevated temperatures. In specimen 17, the angle of the tool was 3°. This angle showed a smaller penetration in the aluminum plates and, consequently, a greater distance from the titanium plate. Thus, the influence of the pin was not visible, as seen in specimen 8. Due to the greater proximity of the pin in specimen 8, the elevated temperatures reached favored the relief of the residual stresses, obtaining smaller values, as compared to specimen 10.

3.7 Aluminum longitudinal residual stress

In the central region of the upper part of the weld, the maximum stress observed was 346 MPa for 1100 rpm, feed of 20 mm/min, and angle of 3°. The minimum stress observed was of 24 MPa for 1300 rpm, feed of 30 mm/min, and angle of 2°. The results are shown in Table 2.

The residual stress depth profile showed a decreasing curve. On the surface of the specimen, all the profiles presented tensile stress and, as the depth increased, the stress decreased, reaching values close to zero, becoming compressive in some cases. The tensile stresses arise

from the mechanical work the surface of the specimen is submitted to, and from the elevated temperatures, due to the contact of the shoulder with the plates. Figure 16 shows the behavior of the stress along the depths of specimens 25, 7, 24, and 8, in which they had the same welding angle equal to 1°. The welding parameters for the Fig. 14 are resumed in the Table 3.

The behavior of the stress profile for the 3° angle was like that found in the 1° angle profile (Fig. 15). Test 8 presented low voltage because a crack was identified in the region near the measurement. The welding parameters for the specimens of Fig. 17 are resumed on Table 4.

The profiles of the tests with extreme conditions showed a tendency similar to the previous results (Fig. 18). The parameters were not favorable to the weld metal consolidation process and contributed to forming internal voids. The welding parameters for the specimens of Fig. 18 are resumed on Table 5.

The central point shown in Fig. 19 did not present curves similar to the previous cases. One of the causes was the formation of internal defects visualized in the weld. Another possible cause was the variation in the burr thickness. The welding parameters for the specimens of Fig. 19 are resumed on Table 6.

The cross-sectional profile of the residual stress (Fig. 20) was performed on specimens 8 and 17. In specimen 17, it was possible to visualize the profile formation in M, verified in the literature. In the mixing zone, due to elevated temperatures and plastic deformation from the pin action, the residual stress in the region was high. In the TMAZ region, the temperatures

Table 4 Resume of the welding parameters for Fig. 17

Test	Specimen number	Rotation, n (rpm)	Travel speed, f (mm/min)	Tilt angle, α (°)
5	10	1100	20	3
6	9	1500	20	3
7	17	1100	40	3
8	22	1500	40	3

Source: author

Fig. 18 Surface residual stress for the conditions of the star points

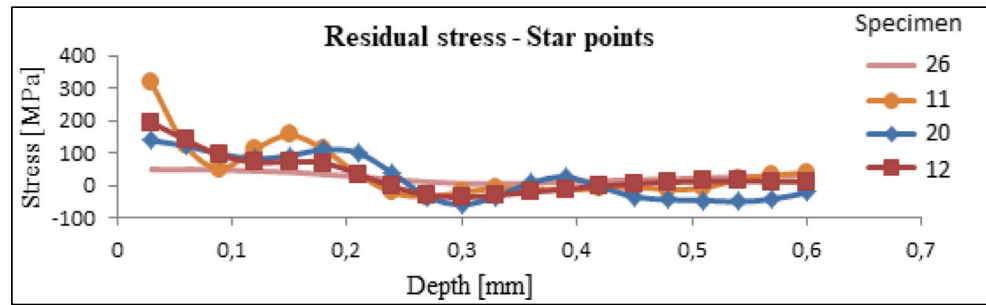


Table 5 Resume of the welding parameters for Fig. 18

Test	Specimen number	Rotation, n (rpm)	Travel speed, f (mm/min)	Tilt angle, α (°)
9	26	1300	30	0.32
11	11	1300	13.18	2
13	20	963.60	30	2
14	12	1636.40	30	2

Source: author

did not reach high values equal to those of the mixing zone. Therefore, the stress in this region is higher. In HAZ, only the influence of temperature occurred and the stress is lower when compared to the mixing zones and TMAZ. In the zone of the base metal, the stress was negative due to the lamination process of the plates. In test specimen 8, the M profile was not observed. In this specimen, near the measurement region, a crack was identified and the stress in the region was thus alleviated.

3.8 Microhardness on the aluminum side

Comparing the result to the base metal, it was possible to obtain a maximum microhardness of 154 HV, corresponding to 85% of AA7475 hardness. Figure 21 shows the microhardness obtained for the specimens and base metals. The microhardness of all specimens resulted in values close to AA7475.

The microhardness showed a R^2 of 0.67, where the feed was the only parameter that presented a level of significance p of 0.05.

By analyzing the response surface between the feed and the angle, it was possible to verify that, for feeds between 12 and 30 mm/min, the angle influenced the microhardness. High angles resulted in low microhardness. For feeds greater than 30 mm/min, the angle had no significant influence. The influence of the angle is related to the area of contact of the shoulder in the plate. Larger angles show a smaller area of contact of the shoulder and, consequently, a lower mechanical work on the surface, which resulted in lower microhardness values. The influence of the feed is related to the support force. High feeds resulted in high supporting force. A greater support force represents a greater mechanical work on the surface and, consequently, higher values of microhardness.

The transverse profile of the microhardness on the aluminum side showed the M profile. Figure 22 shows

Fig. 19 Surface residual stress for the conditions of the central points

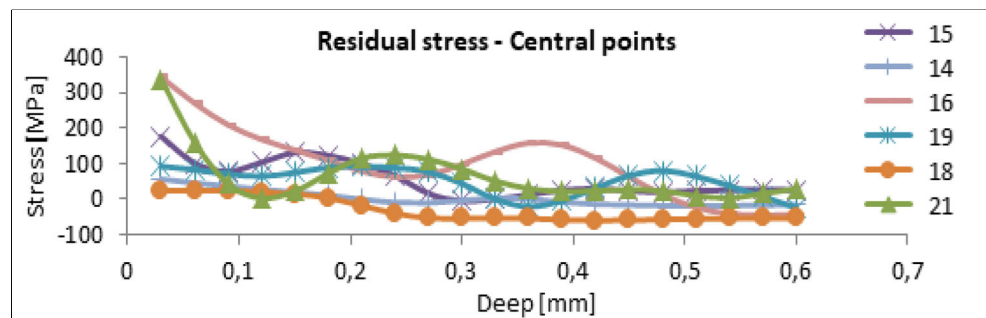
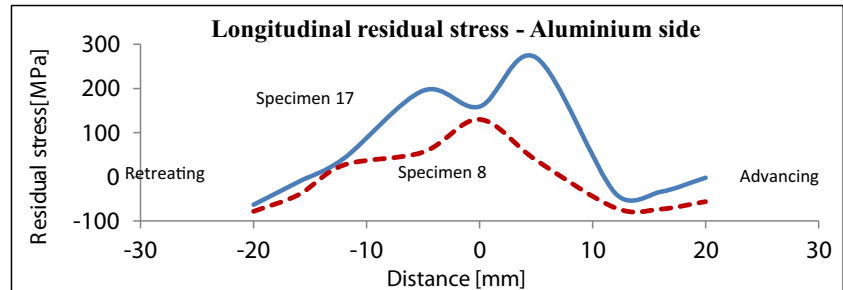


Table 6 Resume of the welding parameters for Fig. 19

Test	Specimen	Rotation, n (rpm)	Travel speed, f (mm/min)	Tilt angle, α ($^\circ$)
15–20	15, 14, 16, 19, 18, 21	1300	30	2

Source: author

Fig. 20 Profile of residual stress at different distances of the weld line. Source: author



the profile obtained. In test specimen 8, the contact of the tool occurred on the titanium plate and, because of this, the pin region suffered greater influence, as compared to specimen 17, where, due to the angle of 3° , the penetration of the tool was lower.

3.9 Microhardness on the titanium side

The maximum microhardness obtained was 384 HV and the minimum was 333 HV, a ratio of 1.05 and 0.91, respectively, when compared to the base metal. Figure 23 shows the result of the microhardness.

For the comparison between response surface of microhardness and temperature, it was possible to see a correlation where high microhardness corresponds to low temperature area. Figure 24 illustrates the response surface of microhardness (a) and temperature (b).

The titanium microhardness profile (Fig. 25) presented the same microhardness profile as aluminum. In the regions near the pin, where the elevated temperatures occurred, the microhardness showed low values, demonstrating a relation on the surfaces of response between titanium microhardness and temperature. In specimen 8,

due to the contact of the tool with the titanium plate, the profile presented inferior values as compared to specimen 17. This results from the temperature the specimen reached in this region being higher than that reached by specimen 17, which had a larger angle, with less approximation of the tool with the titanium plate.

3.10 Tensile testing analysis

The maximum strength reached in specimen 18 was 12 kN for the parameters of 1300 rpm, feed of 30 mm/min, and angle of 2° , obtaining a soldering efficiency of 119% in relation to the base material of the least breaking force (AA2024). In addition to this specimen, specimens 9 and 12 showed a fracture load of 11 and 10 kN, respectively, both above the load of the base material AA2024. The high efficiency should be the effective consolidation of the weld between the aluminum and titanium alloys. Another factor was the absence of defect in these specimens. The result of the test is shown in Fig. 26.

The minimum force was 2.7 kN for 1300 rpm, feed of 47 mm/min, and angle of 2° . Due to weld defects,

Fig. 21 Vickers microhardness of upper region of specimens. Source: author

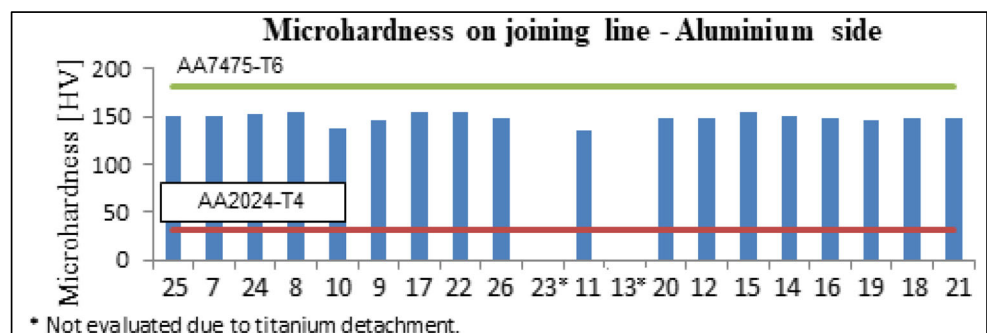


Fig. 22 Microhardness in the cross-section of the aluminum side. Source: author

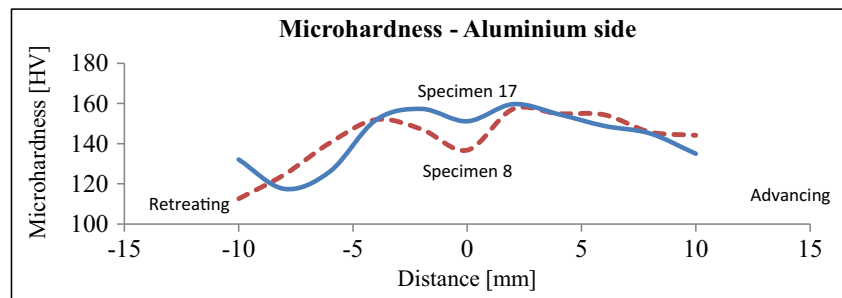
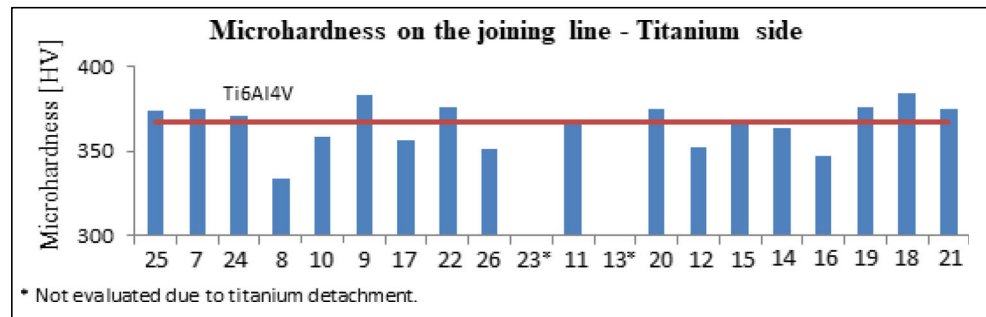


Fig. 23 Vickers microhardness obtained on the titanium side. Source: author



mainly in the formation of voids, some specimens showed low rupture loading.

The displacement force curve shown in Fig. 27 demonstrates the tensile behavior of specimen 18, which obtained the highest resistance limit among the specimens tested. In the figure, the specimen is compared with the force curve by the displacement of the base metals without processing. The behavior of the weld was similar to that of base metal AA7475, reaching

92% of the maximum strength of AA7475 and 119% of AA2024.

4 Conclusions

- It was possible to perform a tri-dissimilar linear friction weld between aluminum and titanium alloys without defects in most of the selected parameters.

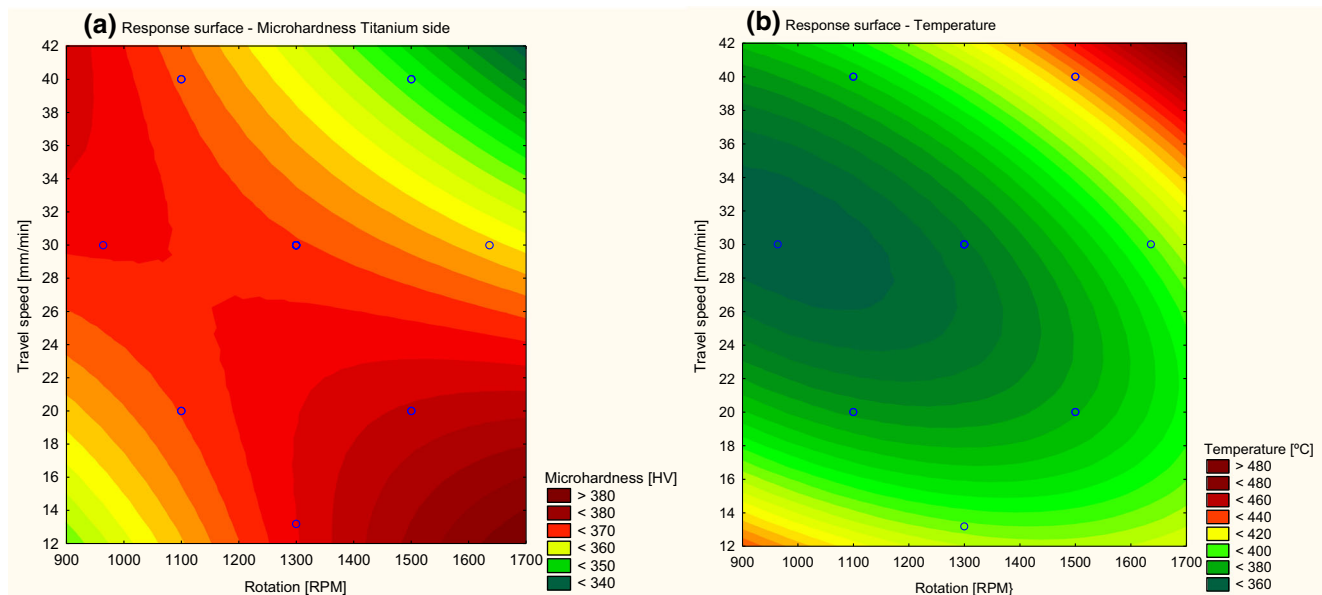


Fig. 24 Response surface a microhardness and b temperature. Source: author

Fig. 25 Microhardness in the titanium side cross-section.
Source: author

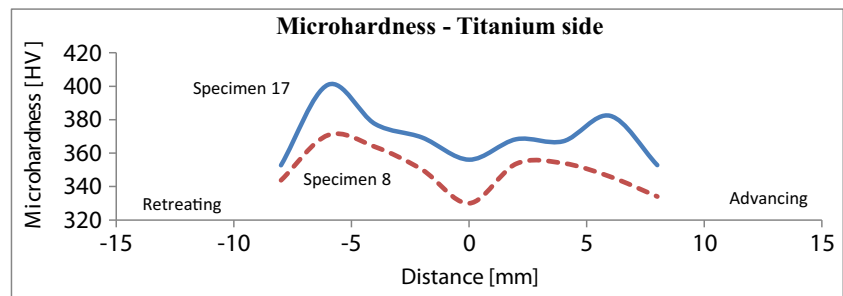
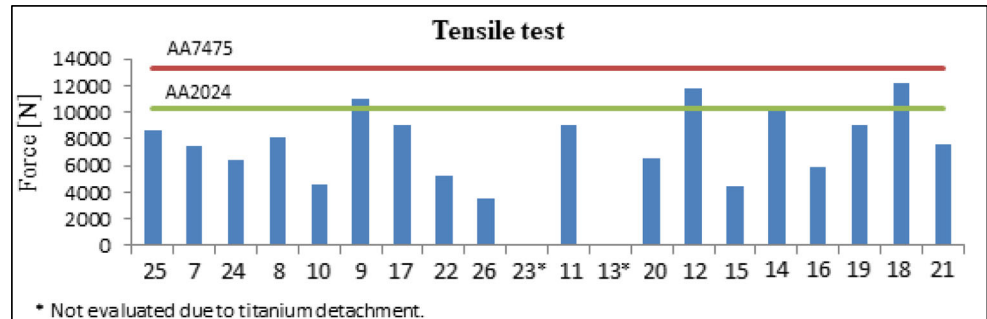
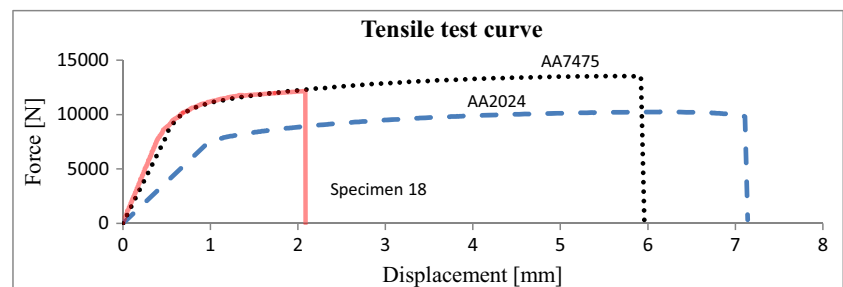


Fig. 26 Results of the tensile tests. Source: author



- The tool positioning angle directly influenced the penetration of the tool in the weld and, consequently, in the analyzed parameters. High angles presented low penetration and angles close to zero presented an irregular mixture. For the 3.68° angle, the titanium plate did not adhere to the weld. The 1° tilt angle condition presented high penetration in the aluminum plate, resulting in the contact with the titanium plate and the 0.36° tilt angle presented an irregular contact of the shoulder with the surface of the aluminum plates, resulting in voids defects.
- In the analysis of the parameters monitored, the support force showed the feed and the tilt angle to exert greater influence. High feeds resulted in high values in the support force and angles close to 2° presented greater support force. The torque was related to the rotation, feed, and angle. Low speeds and high feed rate resulted in high torque. Tilt angles between 1° and 2° resulted in higher torques. The temperature was influenced by the feed and by the angle. Feeds below 18 min/min and above 34 mm/min showed high temperatures. Angles between 1° and 2° presented higher temperatures.
- For analyzing the surface of the aluminum side, the residual stress presented a strong relation with the microhardness, where high residual stresses and low microhardness are present. The profile in M, characteristic of the friction welding between the aluminum alloys studied, was observed in the transverse profile of the residual stress and microhardness.
- The residual stress on the titanium side showed a strong relation with the temperature; results with high residual stresses presented low temperatures. The titanium microhardness did not show a meaningful relationship with the independent parameters. The influence of the pin on the transversal profile of the residual stress and microhardness was observed due to the elevated temperature in the region near the pin. In the residual stress, the region near the pin presented values lower than in the adjacent regions. Regarding microhardness, the regions near the pin presented higher values as compared to the adjacent regions.
- Through the tensile test, welds with resistance limit were verified above the resistance limit of AA2024. This was due to titanium plate, which had the reinforcement function for the weld.

Fig. 27 Force curve by displacement of the tensile test.
Source: author



References

- Akinlabi, E.T., Andrews, A., Akinlabi, S.A., 2014. Effects of processing parameters on corrosion properties of dissimilar friction stir welds of aluminium and copper. *Trans. Nonferrous Metals Soc*
- Cavaliere, A., De Santis, F., Panella, A., Squillace, (2009). Effect of welding parameters on mechanical and microstructural properties of dissimilar AA6082eAA2024 joints produced by friction stir welding. *Materials and Design*
- Chen, Y. C., Nakata, K., 2009. Microstructural characterization and mechanical properties in friction stir welding of aluminum and titanium dissimilar alloys. *Materials and Design*
- European Aluminium Association, 2017. *Aluminium in Cars - Unlocking the Light-Weighting Potential*, p. 6. Brussels - Belgium
- Guo, J.F., Chen, H.C., Sun, C.N. Bi, G., Sun, Z., Wei, J.(2014) Friction stir welding of dissimilar materials between AA6061 and AA7075 al alloys effects of process parameters. *Materials and Design*
- Hiller, D. D. J., 2007. Estudo de parâmetros e percursos no processo de soldagem de mistura por atrito (FSW) da liga de alumínio 505. *Dissertação, Universidade Federal do Rio de Janeiro, Rio de Janeiro*
- Hussein, S. A. et al., 2014. The joining of three dissimilar metallic alloys by a single pass friction stir welding. *International symposium on research in innovation and sustainability, Malacca—Malaysia*
- Khodir, S.A., Shibayanagi, T. (2008) Friction stir welding of dissimilar AA2024 and AA7075 aluminum alloys. *Mater. Sci. Eng. B*
- Kim YG et al (2006) Three defect in friction stir welding of aluminum die casting alloy. In: *Material Science and Engineering A*
- Kusuda, Y., 2013. Honda develops robotized FSW technology to weld steel and aluminum and applied it to a mass-production vehicle. *Industrial Robot: An International Journal*
- Li, B., Zhang, Z., Shen, Y., Hu, W., Luo, L., 2014 Dissimilar friction stir welding of Ti6Al4V alloy and aluminum alloy employing a modified butt joint configuration: influences of process variables on the weld interfaces and tensile properties. *Materials and Design*
- Liu, X., Lan, S. Ni, J., 2014. Analysis of process parameters effects on friction stir welding of dissimilar aluminum alloy to advanced high strength steel. *Materials and Design*
- Mishra, R. S., Ma, Z. Y., 2005. Friction stir welding and processing. *Mater Sci Eng: R: Reports*, 50, n. 1–2, p. 1–78
- Najafkhani, A., Zangeneh-Madar, K., Abbszadeh, H., 2010. Evaluation of microstructure and mechanical properties of friction stir welded copper/316L stainless steel dissimilar metals. *International Journal of Iron & Steel Society of Iran*
- Prater T (2014) Friction stir welding of metal matrix composites for use in aerospace structures. *Acta Astronautica* 93:366–373
- Rodriguez, R.I, Jordon, J.B., Allison, P.G., Rushing, T., Garcia, L., 2015. Microstructure and mechanical properties of dissimilar friction stir welding of 6061-to-7050 aluminum alloys. *Materials and Design*
- Shah, S., Tosunoglu S 2012. Friction stir welding: current state of the art and future prospects. *The 16th world multi-conference on cybernetics and informatics*
- Salih, A. S. et al., 2015 A review of friction stir welding of aluminium matrix composites. *Materials and Design*
- Song Y. et al., (2014) Defect features and mechanical properties of friction stir lap welded dissimilar AA2024eAA7075 aluminum alloy sheets. *Materials and Design*
- Thomas, W. M. et al. 1991. Patent Application No. 9123978.8
- Zapata J., Toro M., Lopez D., 2016 Residual stresses in friction stir dissimilar welding of aluminum alloys. *Journal of Materials Processing Technology*